COBEM 2021 26th International Congress of Mechanical Engineering
November 22-26, 2021, Virtual Congress, Brazil
ABCM Associação Brasileira de Engenharia e Ciências Mecânicas

# COBEM-2021
# VERIFICATION OF SYMMETRY AND CONVERGENCE TOWARDS STEADY-STATE OF WENO SCHEMES

**Rafael H. Olindo de Oliveira**
**Luciano K. Araki**
Postgraduate Program in Mechanical Engineering, Federal University of Paraná, Curitiba, Brazil
roliveiraengmec@gmail.com, lucaraki@ufpr.br

**Nicholas Dicati P. da Silva**
Department of Mechanical Engineering, Maringá State University, Maringá, Brazil
ndicati@gmail.com

**Rafael B. de R. Borges**
Mathematics and Statistics Institute, Rio de Janeiro State University, Rio de Janeiro, Brazil
rafael.borges@ime.uerj.br

*Challenging engineering problems require high resolution and accuracy, as in the case of solving hyperbolic partial differential equations whose solutions may contain discontinuities, even when initial conditions are smooth, or when dealing with the interface between fluids. To deal with such complex flows, WENO schemes are broadly used in CFD simulations. This class of schemes aims to avoid the stencils with a discontinuity, reaching a high resolution. However, the higher the accuracy order, the lower the false diffusion is, which can intensify the round-off error perturbation effects, mainly in Euler equations, because there is no source of diffusion in the model. These perturbations can lead to symmetry breaking in symmetric problems, explained by the arithmetic floating-point non-associativity of algorithms. In this sense, the goal of this work is to evaluate the residuum and the symmetry preserving behavior for recent WENO schemes: WENO-Z+, WENO-EJS, WENO-EZ, WENO-MR, and WENO-MZ. They were implemented along with the positivity preserving Lax-Friedrichs splitting and the 3rd-order strong stability preserving Runge-Kutta in five test problems. The first one is a smooth quasi-1D nozzle flow to check the accuracy, and the second one was performed to test those schemes facing discontinuities produced by a normal shock wave. The third one is 2D and aims to contrast the performance with an oblique shock reflection problem. The last two are the Rayleigh-Taylor instability and the implosion problems, which present complex flow structures and are interesting test cases for symmetry. For the first two, the $L^1$, $L^2$ and $L^\infty$ residuum norms were evaluated and, particularly in the first one, the accuracy order is presented based on the exact solution. For the last two, those same norms were evaluated for the difference between conservative vectors on each side of the symmetry line to verify solution symmetry. As a result, only WENO-MR and WENO-EJS settled down in the nozzle flow presenting a normal shock wave. For the oblique shock reflection, only the WENO-MR was able to settle down. For the Rayleigh-Taylor problem, one can see a good hold of symmetry to every scheme but WENO-Z+. For the implosion problem, the WENO-MR and WENO-EJS presented a good hold of symmetry, while WENO-Z+ and WENO-MZ showed the highest residuum's norms. Even though not all WENO schemes reached the machine error level, all of them were able to get the steady-state solution.*

***Keywords:*** *CFD, WENO, Symmetry preserving.*

## 1. INTRODUCTION

Simulations involving shock-waves and its interactions in some compressible supersonic nozzle flows or multiphase flows, with interactions between two interfaces, are of particular interest in industrial and design applications and high-order and high-resolution methods are required in order to achieve reliable numerical solutions. For this reason, WENO schemes are broadly used in CFD simulations and are still being improved (Hong *et al.*, 2020).

The original WENO scheme takes a convex combination of a collection of stencils attributing lower weights values to the less smooth ones, instead of getting the smoothest stencil like the ENO method. As a result, this WENO scheme was able to improve 1 accuracy order than the ENO scheme based on the same stencil's collection in smooth regions (Liu *et al.*, 1994).

By changing the smoothness indicator, the former WENO based on a collection of r stencils could have its accuracy improved from r+1 to 2r-1 accuracy order, making use at the most all those stencil information (Hong *et al.*, 2020; Jiang

and Shu, 1996). Therefore, WENO-JS yielded a more efficient computational scheme. However, some issues about the loss of accuracy order in critical points has arouse interest. The fifth-order scheme reaches only third-order at critical points of smooth solutions.

It is demonstrated that WENO-JS smoothness indicator does not satisfy some accuracy constraints which are necessary conditions for having convergence to the theoretical accuracy order in critical points (Henrick *et al.*, 2005). Also in this work is presented a mapped formulation of the fifth order WENO-JS weights, whose imposed conditions lead to a more accurate scheme at critical points of smooth regions.

Another smoothness indicator without mapping functions was developed in Borges *et al.* (2008), also known as WENO-Z, which achieved lower CPU cost than WENO-M and recovered optimal order at critical points. There, the weights values assume larger values for the discontinuous stencils when compared with WENO-M and the Classical WENO. Beside that, it was able to decrease the spurious dissipation in stencils with a discontinuous in its neighborhood.

Despite of these improvements, neither WENO-M nor WENO-Z present a symmetric error behavior around a discontinuity. When error perturbations are propagated through the solution, a long term simulation may became asymmetric even for a symmetric problem. Besides that, some issues of asymmetry are also noticed due to non-associativity of floating-point arithmetic (Fleischmann *et al.*, 2019).

A symmetry-preserving behavior was achieved by adapting the Henrick mapping of WENO-M and by building a weights mapping function for WENO-Z imposing a condition to its derivatives, i.e. satisfying $g'(0)_k = 0$. The reformulated WENO-M and the mapped WENO-Z were able to get rid of distortions observed for long term simulations with the former schemes (Hong *et al.*, 2020).

The previous WENO schemes do not make use of all stencil information when there is nonsmooth regions inside of. In order to avoid wasting of computational resources and increase the accuracy order in this case, the embedded WENO strategy was proposed in van Lith *et al.* (2017). It improves the usage of cell information on the discretization, allowing higher accuracy order when non-smooth points are located in the stencil's extrema, such that a $O(h^5)$ scheme can achieve $O(h^4)$ in non-smooth ones.

Once time discretization errors may overlap the accuracy order of WENO spatial discretization, high-order TVD Runge-Kutta is employed. Nevertheless, although it has shown good performance when applied for transient benchmark problems, for steady-state problems residuals may not reach machine error, hanging at truncation error level.

After presenting the main aspects of WENO schemes and issues in this introduction, in the following sections we show the methodology and results of our numerical experiments performed in this work.

## 2. NUMERICAL METHODS

To solve the numerical problems, we employed the Euler equations

$$\boldsymbol{U}_t + \boldsymbol{F}(\boldsymbol{U})_x + \boldsymbol{G}(\boldsymbol{U})_y = \boldsymbol{S}(\boldsymbol{U}), \tag{1}$$

with

$$\boldsymbol{U} = \begin{bmatrix} \rho \\ \rho u \\ \rho v \\ E \end{bmatrix}, \ \boldsymbol{F}(\boldsymbol{U}) = \begin{bmatrix} \rho u \\ \rho u^2 + p \\ \rho uv \\ u(E+p) \end{bmatrix}, \ \boldsymbol{G}(\boldsymbol{U}) = \begin{bmatrix} \rho v \\ \rho uv \\ \rho v^2 + p \\ v(E+p) \end{bmatrix}, \tag{2}$$

where $\rho$ is the density, $u$ and $v$ are the $x$ and $y$ velocities, $E$ is the total energy per unit volume, $p$ is the pressure, and $\boldsymbol{S}$ is a source term that depends on the numerical problem.

The Euler equations were discretized using a Finite Difference conservative scheme Shu and Osher (1988)

$$\frac{d\boldsymbol{U}_{i,j}(t)}{dt} = -\frac{1}{\Delta x}\left(\hat{\boldsymbol{F}}_{i+1/2,j} - \hat{\boldsymbol{F}}_{i-1/2,j}\right) - \frac{1}{\Delta y}\left(\hat{\boldsymbol{G}}_{i,j+1/2} - \hat{\boldsymbol{G}}_{i,j-1/2}\right) + \boldsymbol{S}(\boldsymbol{U}_{i,j}), \tag{3}$$

and a positivity preserving Lax–Friedrichs flux splitting Zhang and Shu (2012).

$$\boldsymbol{F}^{\pm}(\boldsymbol{U}_{i,j}) = \frac{1}{2}\left(\boldsymbol{U}_{i,j} \pm \frac{\boldsymbol{F}(\boldsymbol{U}_{i,j})}{\alpha_x}\right), \tag{4}$$

where $\Delta x = \Delta y$ are the mesh sizes, $\alpha_x = \max_{\boldsymbol{U}} \max_{m} |\lambda_m(\boldsymbol{U})|$, and $\lambda_m$ are the eigenvalues.

To approximate the numerical flux, e.g. the $\hat{\boldsymbol{F}}_{i+1/2,j}$, we employed five WENO schemes: Embedded Jiang–Shu and WENO-Z van Lith *et al.* (2017), WENO multi-resolution Zhu and Shu (2018), mapped WENO-Z Hong *et al.* (2020), and WENO-Z$^+$ Acker *et al.* (2016).

As numerical integration, we employed the third-order strong stability preserving Runge–Kutta Shu (1998)

$$\begin{aligned} \boldsymbol{U}^{(1)} &= \boldsymbol{U}^n + \Delta t L(\boldsymbol{U}^n), \\ \boldsymbol{U}^{(2)} &= \frac{3}{4}\boldsymbol{U}^n + \frac{1}{4}\boldsymbol{U}^{(1)} + \frac{1}{4}\Delta t L(\boldsymbol{U}^{(1)}), \\ \boldsymbol{U}^{n+1} &= \frac{1}{3}\boldsymbol{U}^n + \frac{2}{3}\boldsymbol{U}^{(2)} + \frac{2}{3}\Delta t L(\boldsymbol{U}^{(2)}), \end{aligned} \tag{5}$$

were $(1)$ and $(2)$ are the Runge–Kutta steps, $L(\cdot)$ is the spatial approximation, $n$ and are two subsequent time steps, and $\Delta t$ is the time step

$$\Delta t = \min\left[\frac{CFL}{\alpha_x/\Delta x + \alpha_y/\Delta y}, \min\left(\Delta x, \Delta y\right)^{5/3}\right], \tag{6}$$

where $\alpha_y$ is computed similarly to the $\alpha_x$ for the $y$-direction.

When solving 2D problems the $y$-direction flux is discretized in a similar way as the $x$-direction flux. For simplicity, we use the analytical or exact solution at the ghost points, periodic, or constant boundary treatment. Thus, we can focus on the WENO schemes.

## 3. TEST PROBLEMS

### 3.1 QUASI-ONE-DIMENSIONAL NOZZLE FLOW

The Quasi-1D nozzle flow is our first problem, and despite being 1D, it can model smooth varying nozzle profiles. We use the (1) with 1D terms and

$$\boldsymbol{S}(\boldsymbol{U}) = -\frac{A_x}{A}\begin{bmatrix} \rho u \\ \rho u^2 \\ u(E+p) \end{bmatrix}, \tag{7}$$

where $A$ is the nozzle area.

As stated in Borges *et al.* (2020), care must be taken when proposing nozzle profiles to the Q1D flows. If the functions describing the profile are not smooth enough, oscillations may appear. For simplicity, we use a parabolic profile

$$r(x) = 3(x - x_{th})^2 + r_{th}, \tag{8}$$

were $r$ is the nozzle radius, $x_{th} = 0.1\ m$ is the throat position, and $r_{th} = 0.01\ m$ is the throat radius.

Detailed theoretical and numerical analysis for the Q1D flows can be found in Anderson (2003); Borges *et al.* (2020), including the exact solution. We modeled an air flow with $0.2\ MPa$ as total pressure and $800\ K$ as total temperature. For the adiabatic flow, we imposed an exit pressure of $101.325\ kPa$.

Here, we are interested in the WENO schemes verification and the residuum behavior for discontinuous solutions. As shown in Tab. 1, the WENO-Z$^+$ reached its fifth-order design accuracy. For brevity, we only show the accuracy analysis for the WENO-Z$^+$, since the other schemes behaved similarly.

Table 1: WENO-Z$^+$ accuracy results for the Q1D isentropic flow.

| $\Delta x$ | $L^1$ norm | Order | $L^2$ norm | Order | $L^\infty$ norm | Order |
|---|---|---|---|---|---|---|
| $0.2/20$ | 1.91E-04 | - | 5.44E-04 | - | 2.96E-03 | - |
| $0.2/40$ | 1.92E-05 | 3.32 | 5.94E-05 | 3.19 | 4.19E-04 | 2.82 |
| $0.2/80$ | 2.33E-07 | 6.37 | 7.34E-07 | 6.34 | 3.92E-06 | 6.74 |
| $0.2/160$ | 4.71E-09 | 5.63 | 1.32E-08 | 5.79 | 6.06E-08 | 6.01 |
| $0.2/320$ | 1.19E-10 | 5.31 | 3.46E-10 | 5.26 | 1.80E-09 | 5.08 |

The residuum were computed with

$$\text{Res} = \frac{1}{3N\Delta t}\sum_i \boldsymbol{U}_i^{(n+1)} - \boldsymbol{U}_i^{(n)}. \tag{9}$$

Because of the $\boldsymbol{U}$ third component magnitude, the residuum will not settle down, e.g., near $10^{-15}$ for double precision. We show in Fig. 1 that all WENO schemes settled down nicely after $10^4$ iterations for the smooth problem. However, in Fig. 2 only the multi-resolution WENO and Embedded Jiang–Shu WENO settled down.

As shown in Zhu and Shu (2019), the multi-resolution WENO scheme settles down even in elaborated problems with shocks. Although it can happen, classical WENO schemes will not reach machine error. Furthermore, even not reaching the machine error, classical WENO schemes can reach the steady-state.

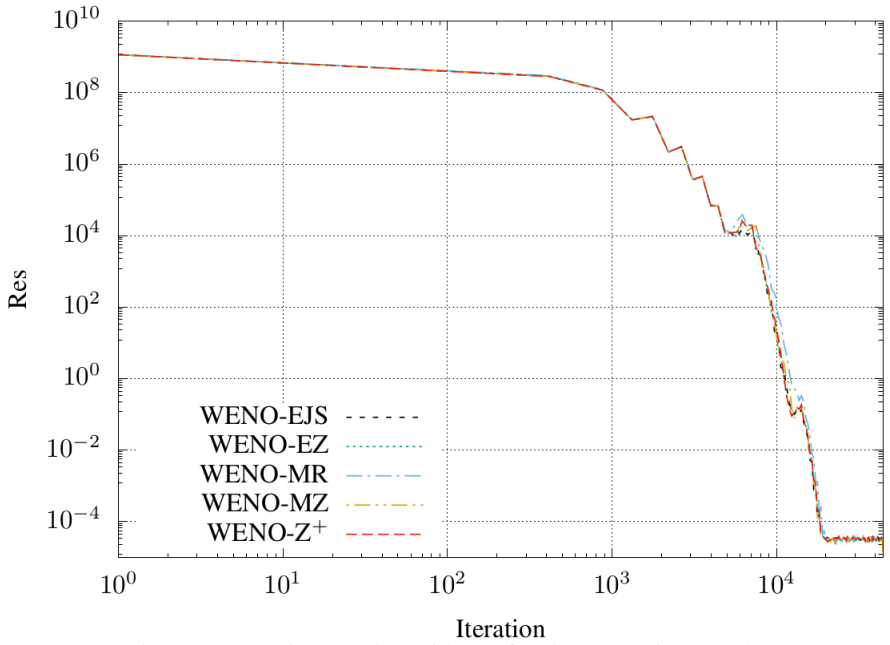


Figure 1: Q1D isentropic residuum for the 320 points mesh.

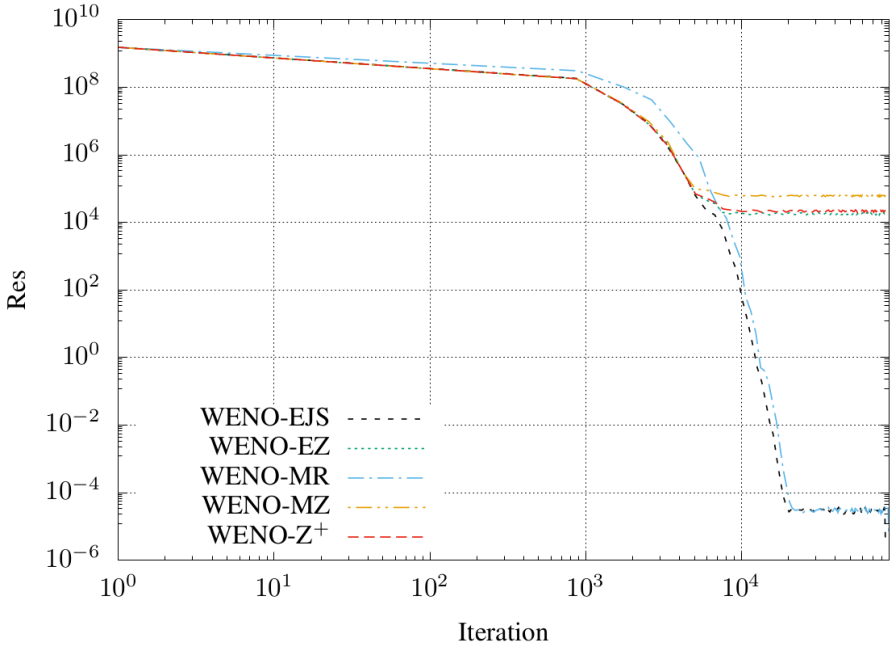


Figure 2: Q1D adiabatic residuum for the 320 points mesh.

### 3.2 SHOCK REFLECTION PROBLEM

Now, we move to 2D problems. The shock reflection problem may also be set up by letting an oblique shock enter the computational domain. Here, we sent a supersonic flow between straight and inclined walls. Because of that, an oblique shock will appear at the beginning of the inclination and reflect at the upper wall.

The domain is $[0, 4] \times [0, 2]$, the inflow is $\rho = 1.23\ kg/m^3$, $p = 101.325\ kPa$, and $M = 2.5$. We use constant values at the inflow boundary, reflexive boundary conditions at straight walls, and supersonic outflow. For simplicity, we set the normal velocity as zero and use pressure and density from the nearest internal point to the inclined wall. We remark that the ILW could easily handle this inclined wall boundary while providing high-resolution Tan *et al.* (2012); Lu *et al.* (2020); Borges *et al.* (2020).

We show a density color map for the WENO-MR in Fig. 3, where we can see that the oblique shock and its reflection

were well captured. For the 2D problems, we rewrite the residuum as

$$\text{Res} = \frac{1}{4P\Delta t}\sum_{i,j} \boldsymbol{U}_{i,j}^{(n+1)} - \boldsymbol{U}_{i,j}^{(n)}, \tag{10}$$

where $P$ is the total mesh points. As shown in the Fig. 4, only the WENO-MR settled down after $10^4$ iterations.

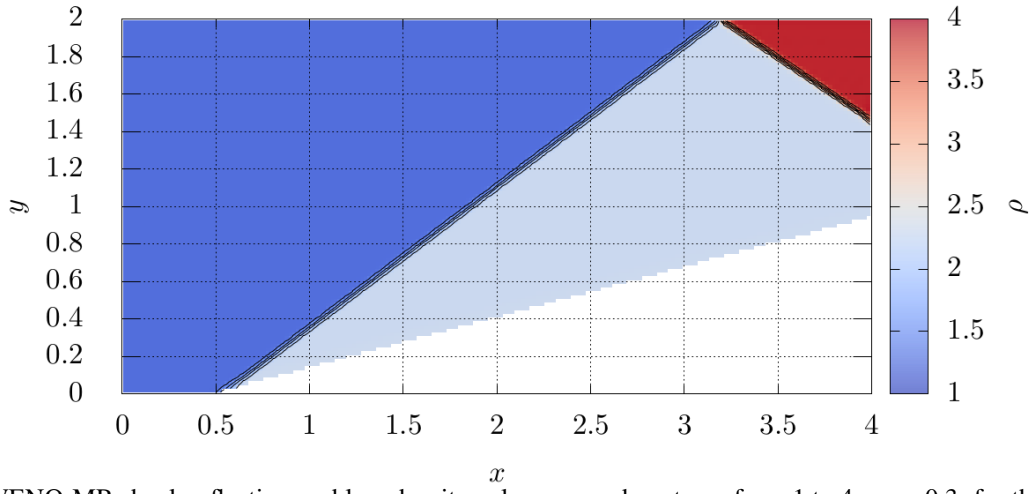


Figure 3: WENO-MR shock reflection problem density color map and contours from 1 to 4 every 0.3. for the $200 \times 100$ points mesh

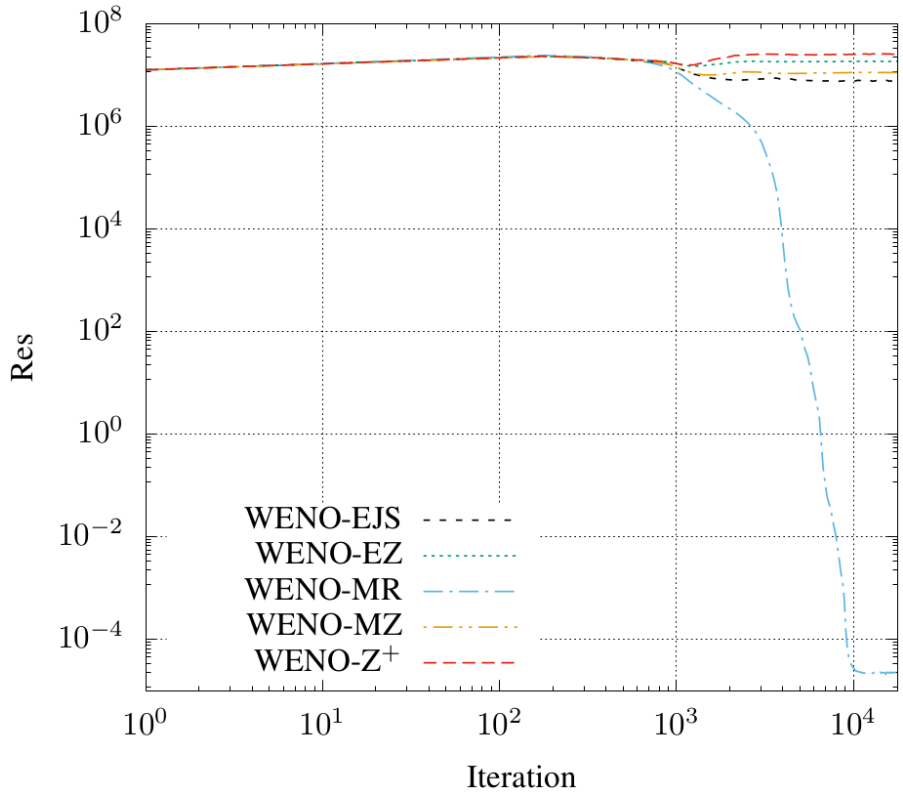


Figure 4: Shock reflection problem residuum for the $200 \times 100$ points mesh

### 3.3 RAYLEIGH–TAYLOR INSTABILITY

The Rayleigh–Taylor instability is an interesting test case, since it has complex flow structures and nonlinear phenomena. It is also a good test case for symmetry. To solve this test case, we used $\boldsymbol{S}(\boldsymbol{U}) = (0, 0, U_1, U_3)^T$. The initial

condition was Acker *et al.* (2016)

$$(\rho_0, p_0) = \begin{cases} (2, 2y+1), & y < 1/2, \\ (1, y+3/2), & y \geq 1/2, \end{cases} \tag{11}$$

$$u_0 = 0, \quad v_0 = -0.025a\cos(8\pi x). \tag{12}$$

The computational domain was $[0, 0.25] \times [0, 1]$, $t = 1.95$, and $\gamma = 5/3$. We applied constant values on the upper and lower boundaries, and reflective boundary conditions on the left and right Acker *et al.* (2016).

We show the $L^1$, $L^2$, and $L^\infty$ norms of the difference between both sides of the symmetry line in Tab. 2, where one can see a good hold of symmetry for the schemes WENO-EJS, WENO-EZ, WENO-MR, and WENO-MZ. Despite presenting higher magnitudes, the WENO-Z$^+$ also has a good representation of flow features, as shown in Fig. 5. The difference between the schemes in the Fig. 5 happens because the WENO-Z$^+$ solutions are more smooth.

Table 2: $L^1$, $L^2$, and $L^\infty$ norms of the difference between both sides of the symmetry line for the Rayleigh–Taylor instability and $100 \times 400$ points mesh.

| Scheme | $L^1$ norm | $L^2$ norm | $L^\infty$ norm |
|---|---|---|---|
| WENO-EJS | $8.87E-14$ | $1.15E-12$ | $4.46E-11$ |
| WENO-EZ | $1.96E-11$ | $2.45E-10$ | $1.42E-08$ |
| WENO-MR | $2.61E-14$ | $3.20E-13$ | $2.24E-11$ |
| WENO-MZ | $7.33E-10$ | $2.03E-08$ | $2.71E-06$ |
| WENO-Z$^+$ | $1.56E-06$ | $2.90E-05$ | $2.07E-03$ |

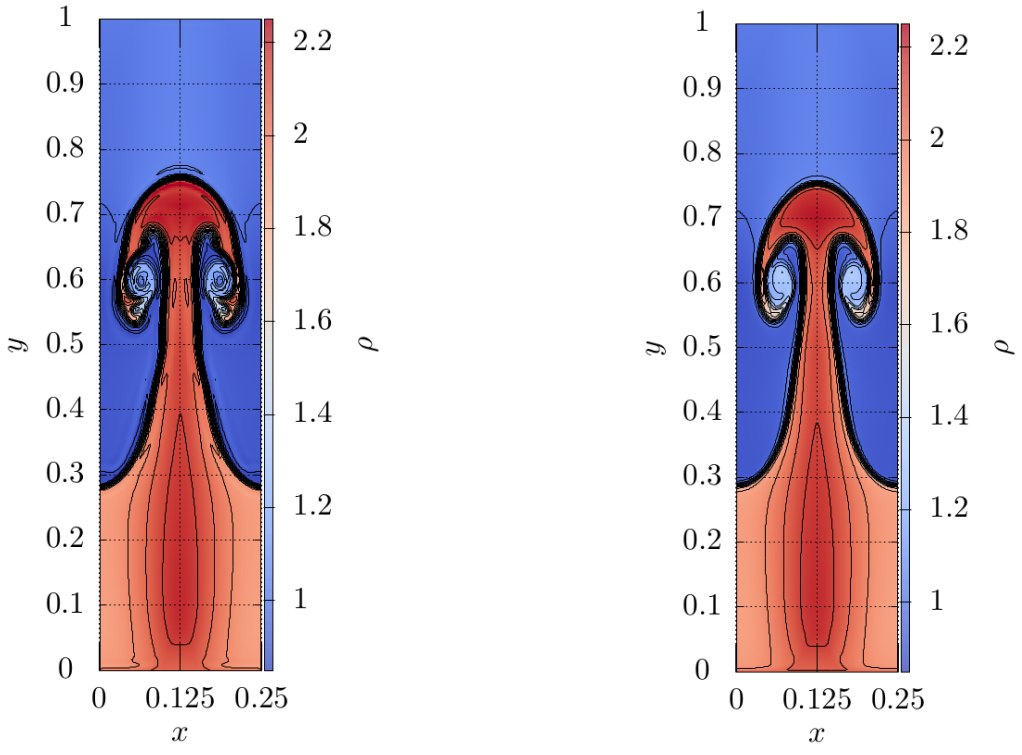


(a) WENO-MR. (b) WENO-Z$^+$.

Figure 5: Rayleigh–Taylor instability density color map and contours from 0.85 to 2.25 every 0.1. for the $100 \times 400$ points mesh.

### 3.4 IMPLOSION TEST CASE

The implosion test has also complex flow structures and nonlinear phenomena. Since all boundaries are treated as reflexive, the nonlinear phenomena interact with each other. Because of the flow configuration, it is also a good test case for symmetry. The problem is set up in a square domain with $0.6\ m$ sides. At $t = 0$, a low-density rotated square box is centered at the origin. For simplicity, one can reduce the domain to $[0, 0.6] \times [0, 0.6]$. As a result, the symmetry line will be $y = x$ Fleischmann *et al.* (2019).

We employed the following initial conditions

$$(\rho, u, v, p) = \begin{cases} (0.124, 0, 0, 0.14) & \text{if} \quad y \leq -x + 0.15, \\ (1, 0, 0, 1) & \text{otherwise.} \end{cases} \tag{13}$$

We show the $L^1$, $L^2$, and $L^\infty$ norms of the difference between both sides of the symmetry line in Tab. 3, where one can see a good hold of symmetry for the schemes WENO-EJS, WENO-EZ, and WENO-MR. The color map and density contours for the $200 \times 200$ points mesh are shown in Fig. 6 and 7 for the WENO-MR and WENO-Z$^+$. Again, the difference between the solution happens because the WENO-Z$^+$ tends to smooth more than the WENO-MR.

Table 3: $L^1$, $L^2$, and $L^\infty$ norms of the difference between both sides of the symmetry line for the implosion test case and $200 \times 200$ points mesh.

| Scheme | $L^1$ norm | $L^1$ norm | $L^1$ norm |
|---|---|---|---|
| WENO-EJS | $2.17E-15$ | $1.43E-14$ | $5.09E-13$ |
| WENO-EZ | $1.40E-09$ | $1.37E-07$ | $4.40E-05$ |
| WENO-MR | $5.15E-16$ | $6.96E-15$ | $4.44E-13$ |
| WENO-MZ | $2.07E-05$ | $4.31E-04$ | $2.90E-02$ |
| WENO-Z$^+$ | $1.49E-06$ | $2.08E-05$ | $1.79E-03$ |

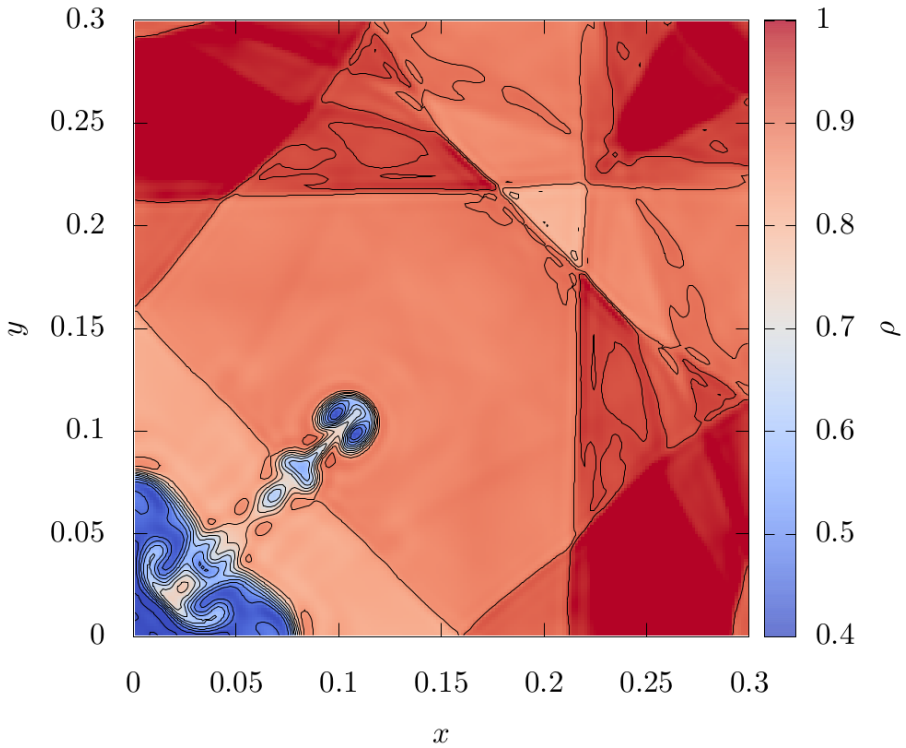


Figure 6: WENO-MR implosion test case density color map and contours from 0.4 to 1 every 0.05 for the $200 \times 200$ points mesh.

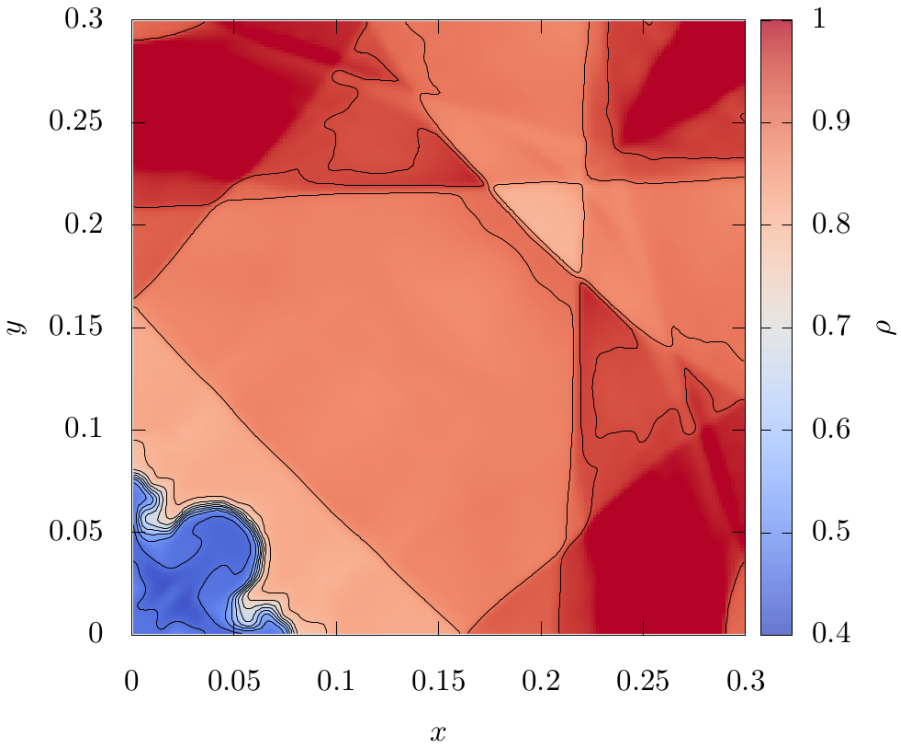


Figure 7: WENO-Z$^+$ implosion test case density color map and contours from 0.4 to 1 every 0.05 for the $200 \times 200$ points mesh.

## 4. CONCLUDING REMARKS

In this work some WENO schemes were tested looking to analyse its symmetry preserving and convergence facing benchmarking problems. Firstly, all the implementations were verified showing convergence to the theoretical order for the quasi-1D isentropic nozzle problem. Changing isentropic quasi-1D nozzle problem to an adiabatic one, the schemes presented different convergence behavior. As one can see, WENO-MR and WENO-EJS spent less iterations to settle down and achieved minor residuum norms than the other ones. For the Shock-reflection problem, only WENO-MR achieved residuum stability after about $10^4$ iterations. Despite of all WENO schemes employed have captured the oblique Shock wave, the multi resolution strategy provided the most converged solution. Regarding the Rayleigh-Taylor symmetry preserving test, all schemes provided symmetric solutions and embedded and multi-resolution strategies led to minor $L^1$, $L^2$ and $L^\infty$ norms. In this case, we highlight the WENO-MR and WENO-EJS which have the minor residuum norm orders. For the implosion problem, we also observe a symmetric solution for all schemes. Once again, WENO-EJS and WENO-MR schemes stood out from the rest regarding the residuum norms calculated, resulting minor norms amongst them all. Therefore, we showed good hold of symmetry for all schemes employed in this work, and the improvements in convergence when Multi-Resolution and Embedded WENO schemes are employed for solving the most of the benchmarking problems. Even not reaching machine error, those schemes can reach steady-state and preserve the solutions symmetry, demonstrating as good strategies for leading with shock-waves and multiphase flows.

## 5. ACKNOWLEDGEMENTS

We would like to thank the CAPES, PG-Mec (Postgraduate Program in Mechanical Engineering) and DEMEC (Department of Mechanical Engineering) of the Federal University of Paraná for their support. The first author was supported by a CAPES scholarship. This study was financed in part by the Coordenação de Aperfeiçoamento de Pessoal de Nível Superior - Brasil (CAPES) - Finance Code 001

## 6. REFERENCES

Acker, F., Borges, R.B.R. and Costa, B., 2016. "An improved weno-z scheme". *Journal of Computational Physics*, Vol. 313, pp. 726–753. doi:https://doi.org/10.1016/j.jcp.2016.01.038.

Anderson, J.D., 2003. *Modern Compressible Flow*. McGraw-Hill, New York, 3rd edition.

Borges, R., Carmona, M., Costa, B. and Don, W.S., 2008. "An improved weighted essentially non-oscillatory scheme for hyperbolic conservation laws". *Journal of Computational Physics*, Vol. 227, pp. 3191–3211.

Borges, R.B.de R., da Silva, N.D.P., Gomes, F.A.A., Shu, C.W. and Tan, S., 2020. "A sequel of inverse Lax–Wendroff high order wall boundary treatment for conservation laws". *Archives of Computational Methods in Engineering*. ISSN 1886-1784. doi:https://doi.org/10.1007/s11831-020-09454-w.

Fleischmann, N., Adami, S. and Adams, N.A., 2019. "Numerical symmetry-preserving techniques for low-dissipation shock-capturing schemes". *Computers & Fluids*, Vol. 189, pp. 94 – 107. ISSN 0045-7930. doi: https://doi.org/10.1016/j.compfluid.2019.04.004.

Henrick, A.K., Aslam, T.D. and Powers, J.M., 2005. "Mapped weighted essentially non-oscillatory schemes: Achieving optimal order near critical points". *Journal of Computational Physics*, Vol. 207, No. 2, pp. 542 – 567. ISSN 0021-9991. doi:https://doi.org/10.1016/j.jcp.2005.01.023.

Hong, Z., Ye, Z. and Ye, K., 2020. "An improved weno-z scheme with symmetry-preserving mapping". *Advances in Aerodynamics*, Vol. 2, No. 1, p. 18. ISSN 2524-6992. doi:https://doi.org/10.1186/s42774-020-00043-w.

Jiang, G.S. and Shu, C.W., 1996. "Efficient implementation of weighted eno schemes". *Journal of Computational Physics*, Vol. 126, No. 1, pp. 202–228. ISSN 0021-9991. doi:https://doi.org/10.1006/jcph.1996.0130.

Liu, X.D., Osher, S. and Chan, T., 1994. "Weighted essentially non-oscillatory schemes". *Journal of Computational Physics*, Vol. 115, No. 1, pp. 200–212. ISSN 0021-9991. doi:https://doi.org/10.1006/jcph.1994.1187.

Lu, J., Shu, C.W., Tan, S. and Zhang, M., 2020. "An inverse lax-wendroff procedure for hyperbolic conservation laws with changing wind direction on the boundary". *Journal of Computational Physics*, p. 109940. ISSN 0021-9991. doi:https://doi.org/10.1016/j.jcp.2020.109940.

Shu, C.W., 1998. *Essentially non-oscillatory and weighted essentially non-oscillatory schemes for hyperbolic conservation laws*, Springer Berlin Heidelberg, Berlin, Heidelberg, pp. 325–432. ISBN 978-3-540-49804-9. doi: 10.1007/BFb0096355.

Shu, C.W. and Osher, S., 1988. "Efficient implementation of essentially non-oscillatory shock-capturing schemes". *Journal of Computational Physics*, Vol. 77, pp. 439–471.

Tan, S., Wang, C., Shu, C.W. and Ning, J., 2012. "Efficient implementation of high order inverse lax–wendroff boundary treatment for conservation laws". *Journal of Computational Physics*, Vol. 231, pp. 2510–2527.

van Lith, B.S., ten Thije Boonkkamp, J.H. and IJzerman, W.L., 2017. "Embedded weno: A design strategy to improve existing weno schemes". *Journal of Computational Physics*, Vol. 330, pp. 529–549. ISSN 0021-9991. doi: https://doi.org/10.1016/j.jcp.2016.11.026.

Zhang, X. and Shu, C.W., 2012. "Positivity-preserving high order finite difference weno schemes for compressible euler equations". *Journal of Computational Physics*, Vol. 231, No. 5, pp. 2245 – 2258. ISSN 0021-9991. doi: https://doi.org/10.1016/j.jcp.2011.11.020.

Zhu, J. and Shu, C.W., 2018. "A new type of multi-resolution weno schemes with increasingly higher order of accuracy". *Journal of Computational Physics*, Vol. 375, pp. 659 – 683. ISSN 0021-9991. doi: https://doi.org/10.1016/j.jcp.2018.09.003.

Zhu, J. and Shu, C.W., 2019. "Convergence to steady-state solutions of the new type of high-order multi-resolution weno schemes: a numerical study". *Communications on Applied Mathematics and Computation*. ISSN 2661-8893.

## 7. RESPONSIBILITY NOTICE

The author(s) is (are) solely responsible for the printed material included in this paper.